Neuroradiology (2021) 63:879–887
https://doi.org/10.1007/s00234-020-02581-y

DIAGNOSTIC NEURORADIOLOGY

Evaluation of cerebral arteriovenous shunts: a comparison of parallel imaging time-of-flight magnetic resonance angiography (TOF-MRA) and compressed sensing TOF-MRA to digital subtraction angiography

Akihiko Sakata[1] · Yasutaka Fushimi[1] · Tomohisa Okada[2] · Satoshi Nakajima[1] · Takuya Hinoda[1] · Peter Speier[3] · Michaela Schmidt[3] · Christoph Forman[3] · Kazumichi Yoshida[4] · Hiroharu Kataoka[4] · Susumu Miyamoto[4] · Yuji Nakamoto[1]

Received: 27 July 2020 / Accepted: 6 October 2020 / Published online: 15 October 2020

Abstract

Purpose Time-of-flight (TOF)-MR angiography (MRA) is an important imaging sequence for the surveillance and analysis of cerebral arteriovenous shunt (AVS), including arteriovenous malformation (AVM) and arteriovenous fistula (AVF). However, this technique has the disadvantage of a relatively long scan time. The aim of this study was to compare diagnostic accuracy between compressed sensing (CS)-TOF and conventional parallel imaging (PI)-TOF-MRA for detecting and characterizing AVS.

Methods This study was approved by the institutional review board for human studies. Participants comprised 56 patients who underwent both CS-TOF-MRA and PI-TOF-MRA on a 3-T MR unit with or without cerebral AVS between June 2016 and September 2018. Imaging parameters for both sequences were almost identical, except the acceleration factor of 3× for PI-TOF-MRA and 6.5× for CS-TOF-MRA, and the scan time of 5 min 19 s for PI-TOF-MRA and 2 min 26 s for CS-TOF-MRA. Two neuroradiologists assessed the accuracy of AVS detection on each sequence and analyzed AVS angioarchitecture. Concordance between CS-TOF, PI-TOF, and digital subtraction angiography was calculated using unweighted and weighted kappa statistics.

Results Both CS-TOF-MRA and PI-TOF-MRA yielded excellent sensitivity and specificity for detecting intracranial AVS (reviewer 1, 97.3%, 94.7%; reviewer 2, 100%, 100%, respectively). Interrater agreement on the angioarchitectural features of intracranial AVS on CS-MRA and PI-MRA was moderate to good.

Conclusion The diagnostic performance of CS-TOF-MRA is comparable to that of PI-TOF-MRA in detecting and classifying AVS with a reduced scan time under 2.5 min.

Keywords Compressed sensing · Parallel imaging · MR angiography · Arteriovenous malformation · Arterial venous fistula

Abbreviations

CS	Compressed sensing
PI	Parallel imaging
MRA	MR angiography
AVM	Arteriovenous malformation
AVF	Arterial venous fistula
DSA	Digital subtraction angiography
AVS	Arteriovenous shunt

Electronic supplementary material The online version of this article (https://doi.org/10.1007/s00234-020-02581-y) contains supplementary material, which is available to authorized users.

✉ Yasutaka Fushimi
yfushimi@kuhp.kyoto-u.ac.jp

[1] Department of Diagnostic Imaging and Nuclear Medicine, Graduate School of Medicine, Kyoto University, 54 Shogoin Kawahara-cho, Sakyo-ku, Kyoto 606-8507, Japan

[2] Human Brain Research Center, Graduate School of Medicine, Kyoto University, Kyoto 606-8507, Japan

[3] Siemens Healthcare GmbH, Allee am Roethelheimpark 2, 91052 Erlangen, Germany

[4] Department of Neurosurgery, Graduate School of Medicine, Kyoto University, Kyoto 606-8507, Japan

SM grade	Spetzler-Martin grade
CVR	Cortical venous reflux
PPV	Positive predictive value
NPV	Negative predictive value

Introduction

Cerebral arteriovenous malformations (AVMs) and arteriovenous fistulas (AVFs) are congenital or acquired diseases characterized by arteriovenous shunt (AVS), which is a direct communication between the arterial and venous circulation without the capillary bed [1, 2]. Patients with AVS carry certain risks of hemorrhagic complications [3, 4]. Moreover, AVS may present with other serious neurological complications such as venous infarction [5, 6]. Delayed diagnosis can thus lead to significant morbidity and mortality [7].

Imaging has played a pivotal role in the management of patients with AVS, since detailed information about the architecture and flow dynamics of AVS is essential for establishing an adequate diagnosis and selecting appropriate therapeutic approaches. Spetzler-Martin (SM) grade is a commonly used classification system for AVM based on eloquence, size, and venous drainage pattern in patients with AVM [8]. Surgery is the treatment of choice for patients with grade 1 or 2 AVM, whereas patients with a higher grade generally undergo multimodal therapy or watchful waiting [9]; either option requires frequent follow-up. Borden proposed a classification for AVF based on the site of venous drainage and the presence or absence of cortical venous drainage [10]. Type I AVF usually shows clinically benign behavior, being either identified incidentally or from minimal symptoms. This type of AVF can be treated conservatively. However, AVFs with cortical venous reflux (type II or III) should receive treatment because they carry an increased risk of hemorrhage or non-hemorrhagic neurological deficit [11].

Digital subtraction angiography (DSA) remains the gold standard in the evaluation of AVS, thanks to its high spatial and temporal resolutions and high interobserver agreement. However, this invasive technique carries a risk of neurological complications and adverse reactions associated with the contrast agent as well as the exposure to ionizing radiation during the procedure. Various non- or less-invasive imaging techniques have thus been applied to the evaluation of AVS [12–22]. Time-of-flight (TOF)-MRA has been the most widely used of these in clinical practice. Past studies have identified TOF-MRA as a sensitive tool for detecting AVS without contrast material [23–28]. Even with parallel imaging (PI), a widely used method for k-space undersampling, TOF-MRA requires a long scanning time, since both wide scan coverage and high resolution are required in the assessment of AVS due to its complex angioarchitecture and hemodynamics. Acceleration factors in PI are limited to low numbers (typically to 2–3×) by the associated increase in noise.

Recently, compressed sensing (CS) has been introduced to clinical settings [29–33]. This technique provides an innovative approach to undersampling k-space, through exploitation of the underlying sparsity in the appropriate transform domain, promising higher acceleration. The source image of TOF-MRA mostly consists of scattered "white" arteries and "black" brain parenchyma, which are thus considered mathematically sparse. In addition, wavelet transformation of MR images makes the resulting image sparse in the wavelet transform domain [34]. The utility of CS has been demonstrated in various MR imaging applications, including TOF-MRA. Previous studies have shown that CS-TOF-MRA provides a clinically acceptable quality of maximum intensity projection images, even with 5× acceleration [33]. With the advantage of this accelerated sequence, an increase of spatial coverage (for example, whole-brain coverage) can be achieved within a clinically acceptable scan time.

CS-TOF-MRA has been successfully applied to the evaluation of different kinds of vascular pathologies, including intracranial aneurysm [33], moyamoya disease [31], and arterial stenosis [35–37]. However, to the best of our knowledge, the utility of CS-TOF-MRA in the evaluation of AVS has not been well investigated. In addition, few studies have referred to the concordance between CS-TOF-MRA and other imaging modalities, such as DSA [36]. The current study aimed to determine whether CS-TOF-MRA is useful for AVS in comparison with PI-TOF-MRA and DSA by focusing on detection and evaluation of the angioarchitectural features of AVS.

Methods

Patients

This retrospective study was approved by the local institutional review board, and the need to obtain written informed consent was waived. A total of 153 patients who had undergone both CS-TOF-MRA and PI-TOF-MRA in another prospective study between June 2016 and September 2018 were enrolled in this study (Fig. 1). No subsets of this patient population have not been published in the past with a research focus not presented in the current article. Patients who underwent any treatment during the interval between DSA and MRI (n = 2), or who had scalp AVM (n = 1) or AVF (n = 1) were excluded. We then excluded 1 patient with AVF diagnosed based solely on MRI findings from the following analyses because no DSA was performed for this patient. We also excluded 92 patients without evidence of AVS who did not undergo DSA or CTA within 1 year of the MRI examination.

Analysis 1, detection of intracranial AVS First, we assessed the accuracy of CS-TOF-MRA and PI-TOF-MRA to detect intracranial AVS. We chose negative controls, which consisted of patients without any evidence of AVS confirmed on DSA or CTA

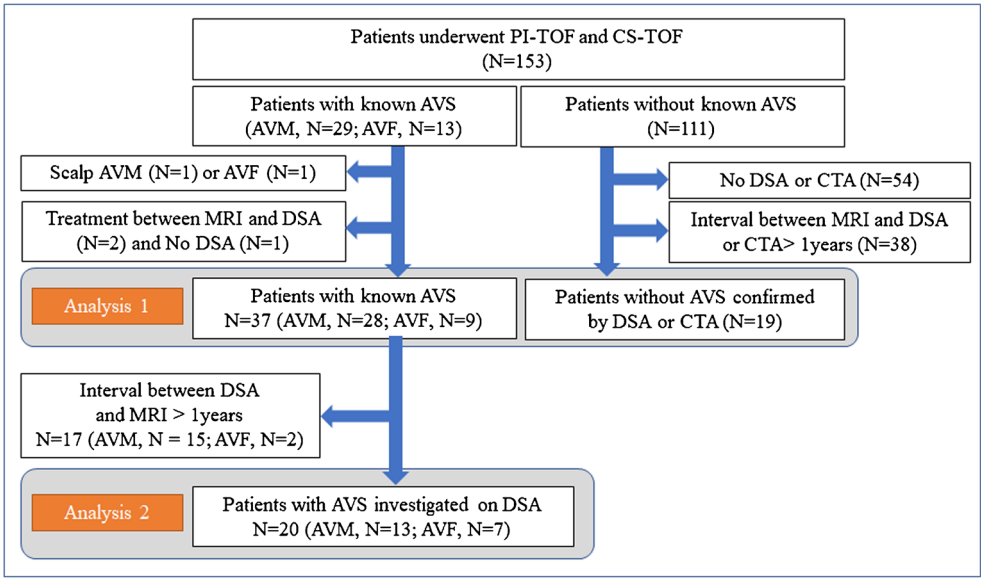

Fig. 1 Flow diagram for inclusion in and exclusion from this study. Note that analysis 1 represents detection of AVS, and analysis 2 represents analysis for AVS angioarchitecture

($n = 19$) which were performed within 1 year of MRI examination. We then also chose patients with known intracranial AVS confirmed by DSA ($n = 37$: AVM, $n = 28$; AVF, $n = 9$) (Fig. 1).

Analysis 2, angioarchitecture analysis of AVS For further analysis of the angioarchitecture of AVS, we included 13 patients with AVM and 7 patients with AVF who underwent MRI examination and DSA within 1 year (Fig. 1) [38]. The median interval between DSA and MRA was 4 days (range, 1–272 days) for patients with AVM and 2 days (range, 1–363 days) for patients with AVF.

MR angiography

We performed all MRA examinations using a 3-T MR imaging system (MAGNETOM Skyra; Siemens Healthcare, Erlangen, Germany) with a 32-channel head coil. Imaging parameters for PI-TOF-MRA were as follows: TR/TE, 20–21/3.7 ms; flip angle, 18–20°; FOV 187.3 × 220 mm^2; matrix size, 328 × 384; slice thickness, 0.7 mm; phase partial Fourier factor, 7/8; number of slabs, 4–5; total slab thickness, 10.2–12.6 cm; acceleration factor, generalized autocalibrating partially parallel acquisition (GRAPPA) 3×; integrated reference scan. Scan time was 4 min 15 s–5 min 19 s, depending on the head and lesion size. Imaging parameters for the prototype CS-TOF-MRA were as follows: TR/TE = 20/3.7 ms; flip angle, 18°; field of view, 187.3 × 220 mm; matrix size, 328 × 384 slice thickness, 0.7 mm; slice resolution, 50%; slice per slab, 44; number of slabs, 5, 180 slices; total slab thickness, 12.6 cm; acceleration factor, 6.5×; and integrated reference scan. Images were automatically interpolated to a 652 × 768 matrix, and final resolution became 0.29 × 0.29 mm. Scan time was 2 min 26 s, while the CS reconstruction time was 5 min 32 s for 10 iterations at an online main console.

DSA examination

All DSA examinations were obtained using an AXIOM-Artis biplane system for conventional angiography (Siemens Healthcare) with Iohexol 300 (Fuji Pharma, Tokyo, Japan). Selective angiographies were acquired using 6–8 ml of the contrast agent at a rate of 2.5–4 ml/s. The images were obtained with 1024 × 1024 matrix and FOV of 29.7 cm. All biplane DSA acquisitions were obtained with temporal resolution ranging from a minimum of 2 to 6 frames/s in standard projections with injection in both ICAs and at least one vertebral artery.

Interpretation of DSA (reference standard)

DSA examinations were interpreted by two board-certified neurosurgeons (K.Y., H.K.) together, both with 26 years of experience. The reported results of those examinations regarding the presence, location, and classification of the AVM and AVF were used as the reference standard.

Detection of AVS (analysis 1)

MRI examinations were interpreted by two board-certified radiologists (Y.F., S.N., with 23 years and 14 years of experiences in neuroradiology, respectively). The readers were asked to identify the presence or absence of AVS in analysis 1. With the source image of TOF-MRA, an AVS was defined as enlarged and dilated serpiginous vessels and/or direct visualization of the fistulous point/nidus [27].

Angioarchitecture analysis of AVS (analysis 2)

The same reviewers evaluated the angioarchitecture of the AVS based on the following criteria: (1) eloquence of adjacent brain, (2) size of nidus, (3) pattern of venous drainage, and (4) SM grade for AVM or Borden grade for AVF based on the pattern of cortical venous reflux (CVR) [10]. If asymmetric dilatation and/or flow-related signal of deep venous structures were observed on TOF-MRA, deep venous drainage was categorized as positive. CVR on TOF-MRA was evaluated based on findings including abnormal dilatation, flow-related enhancement, and presence of medullary or pial veins [16].

Statistical analysis

Sex and age were compared using Fisher's exact test and Wilcoxon ranked sum test between patients with AVS and without AVS.

We calculated standard diagnostic accuracy parameters (sensitivity, specificity, and positive and negative predictive values) for the detection of AVS in analysis 1 and venous reflux of AVM in analysis 2. These probabilities are listed for each reader either on CS-TOF-MRA or on PI-TOF-MRA.

Concordance of the angioarchitectures of AVMs and AVFs between CS-TOF, PI-TOF, and DSA was calculated with unweighted and weighted kappa statistics [13, 14, 25]. Concordance values were interpreted as follows: κ value of 0, poor agreement; κ values of 0.01–0.20, minor agreement; κ values of 0.21–0.40, fair agreement; κ values of 0.41–0.60, moderate agreement; κ values of 0.61–0.80, good agreement; and κ values of 0.81–1, excellent agreement. Values of $p < 0.05$ were considered statistically significant. Statistical analyses were performed using STATA version 13 software (StataCorp, College Station, TX, USA).

Results

Detection of AVS (analysis 1)

Table 1 summarizes the patient characteristics of analysis 1. Nidus size ranges from 13 to 90 mm (median size, 35 mm). Thirty-six of the 37 cases with AVS were correctly identified by reader 1 on both CS-TOF and PI-TOF. All cases with AVS were correctly identified by reader 2 on both CS-TOF and PI-TOF. All 19 cases without AVS were correctly identified as negative for AVS by both readers on each type of MRA. The sensitivity and specificity per image sequence per reader are summarized in Table 2.

Table 1 Participant characteristics (analysis 1)

	AVS (+)	AVS (−)	
Number of patients	37	19	
Mean age (years)	46.6 ± 20.6	55.9 ± 13.4	$p = 0.19$
Female/male	F 17, M 20	F 12, M 7	$p = 0.26$
Diagnosis			
AVMs	28	0	
AVFs	9	0	
Aneurysms untreated	11	10	
Aneurysms treated	0	3	
Stenosis	1	1	
None of the above	0	5	

Angioarchitecture analysis of AVS (analysis 2)

Tables 3 and 4 summarize the patient characteristics of analysis 2.

AVM

Reader 1 correctly detects 4 of the 6 cases with venous reflux, while reader 2 detects 5 out of the 6 cases on CS-TOF and PI-TOF. The sensitivity and specificity of venous reflux per image sequence per reader are summarized in Supplementary Table. As for SM classification, reader 1 correctly classified 8 cases of AVM on CS-TOF and 9 cases on PI-TOF, while reader 2 correctly classified 10 out of 13 cases of AVM on both sequences. The interrater concordance of CS-TOF and PI-TOF for AVM evaluation is shown in Table 5. Intra-rater concordance between CS-TOF-MRA and PI-TOF-MRA for agreement on the SM classification was excellent for both readers (0.84 for reader 1; 1 for reader 2). Interrater reproducibility was also excellent for agreement on the SM classification between both readers. Weighted kappa statistics revealed values of 0.49 (CS-TOF-MRA) and 0.59 (PI-TOF-MRA) for agreement on SM grade between reader 1 and DSA. Weighted kappa statistics revealed a value of 0.68 for agreement on SM grade between reader 2 and DSA. Representative cases are shown in Figs. 2 and 3.

AVF

Intra-rater concordance between CS-TOF-MRA and PI-TOF-MRA was perfect ($\kappa = 1$) for both readers. Both readers correctly classified 6 of the 7 cases of AVF. Interimage sequence reproducibility was moderate ($\kappa = 0.58$, $p = 0.04$) for agreement on Borden classification TOF-MRA and DSA for both readers. A representative case is shown in Fig. 4.

Table 2 Detection of AVS in CS-TOF-MRA and PI-TOF-MRA (95% CI) (analysis 1)

		Shunting	No shunting	Sensitivity	Specificity	PPV	NPV	AUC
Reader 1	CS-TOF positive	36	0	97.3% (85.8–99.9%)	100% (82.4. -100%)	100% (90.3–100%)	94.7% (75.1–99.9%)	0.99 (0.96–1.00)
	CS-TOF negative	1	19					
	PI-TOF positive	36	0	97.3% (85.8–99.9%)	100% (82.4–100%)	100% (90.3–100%)	94.7% (75.1–99.9%)	0.99 (0.96–1.00)
	PI-TOF negative	1	19					
Reader 2	CS-TOF positive	37	0	100% (90.5–100%)	100% (82.4–100%)	100% (90.5–100%)	100% (82.4–100%)	1
	CS-TOF negative	0	19					
	PI-TOF positive	37	0	100% (90.5–100%)	100% (82.4–100%)	100% (90.5–100%)	100% (82.4–100%)	1
	PI-TOF negative	0	19					

PPV positive predictive value, *NPV* negative predictive value

Discussion

The current study evaluated the diagnostic accuracy of whole-brain CS-TOF-MRA 6.5× for detecting AVS in comparison with PI-TOF-MRA, using DSA as the reference standard. Our results showed that CS-TOF-MRA is an effective tool for detecting and classifying intracranial AVS, even within the reduced scan time under 2.5 min.

We demonstrated excellent performance of CS-TOF-MRA for delineating AVS with high sensitivity and specificity. This was in line with past studies showing TOF-MRA as a versatile tool for detecting AVS. Past studies have reported that clinical MRA including TOF-MRA was useful in the detection of AVS with 90–91.7% sensitivity and 94.4–100% specificity [25, 27]. Regarding the fact that extracranial vessels, such as the occipital and middle meningeal arteries, often feed intracranial AVF, MRA of the whole brain at high resolution would be optimal for assessing AVF. In clinical practice, however, TOF-MRA usually provides limited spatial coverage due to the long scan time, which may hinder the detection of AVS. In fact, evaluation of AVF was inadequate in 9% of patients because the shunt site was outside the image volume on TOF-MRA [24]. On the other hand, CS-TOF-MRA has its own advantage of a wide-scan volume coverage within a short scan time. In the current study with CS-TOF-MRA, whole-brain coverage can be achieved within 2.5 min, making this totally feasible as a clinical routine. CS-TOF-MRA has become a clinically useful image sequence thanks to this short scan time, and the large scanning coverage would be particularly beneficial in screening for AVS.

Our study also demonstrated that the intermodality agreement of CS-TOF-MRA with DSA as the reference standard was moderate to good in evaluating the SM grade of AVM. Our result was in accordance with a past study that reported intermodality agreement on AVM characteristics between TOF-MRA and DSA as moderate when rated by an experienced neuroradiologist [13]. We also found that CS-TOF-MRA was useful not only for detection but also for evaluation of AVF in terms of Borden classification, which is based upon the site of venous drainage and the presence or absence of cortical venous drainage [10]. Schubert et al. found that intermodality agreement of the Borden classification between clinical MRA and DSA varied from 0.2 to 0.58 in 6 patients with AVF [25], consistent with our results. The good

Table 3 Characteristics of patients with AVM (analysis 2)

Sex	Age	Location	Eloquence	Venous Reflux	SM grade	History of ICH	Size (mm)
M	16	Hypothalamus	1	1	3	(+)	13
F	36	Right parietooccipital	1	0	2	(−)	24
M	50	Left temporal	1	1	4	(−)	48
M	54	Left frontal	0	0	1	(+)	18
M	70	Cerebellar vermian	0	1	2	(+)	16
F	19	Left parietal	0	0	1	(−)	23
F	46	Right frontal	0	1	4	(−)	34
M	30	Right temporal	0	0	3	(+)	62
M	43	Right frontal	0	0	1	(+)	15
F	11	Right parietooccipital	1	0	3	(−)	36
M	16	Left occipital	1	1	4	(−)	58
F	43	Right frontal	0	1	2	(−)	26
M	34	Right temporo-occipital	0	0	1	(+)	28

SM Spetzler-Martin, *ICH* intracranial hemorrhage

Table 4 Patient characteristics of AVF (analysis 2)

Sex	Age	Location	Venous reflux	Borden classification
M	68	Left anterior condylar confluence	0	1
M	70	Right cavernous sinus	0	1
M	73	Tentorial	1	3
M	74	Anterior cranial base	1	3
F	51	Left TSSJ	0	1
F	71	Left anterior condylar confluence	0	1
F	77	Left TSSJ	0	1

TSSJ transverse sinus-sigmoid sinus junction

Table 5 Interrater reproducibility of CS-TOF-MRA and PI-TOF-MRA for characterization of AVM (95% CI)

		CS-TOF vs PI-TOF	CS-TOF vs DSA	PI-TOF vs DSA
Rater 1	Eloquence	1	1	1
	Nidus size	0.84 (0.55–1.00)	0.71 (0.58–0.83)	0.85 (0.68–1.00)
	Deep venous return	1	0.68 (0.3–1.00)	0.68 (0.3–1.00)
	SM grade	0.9 (0.78–1.00)	0.49 (0.35–0.78)	0.59 (0.35–0.86)
Rater 2	Eloquence	1	1	1
	Nidus size	1	0.85 (0.71–1.00)	0.85 (0.73–1.00)
	Deep venous return	1	0.84 (0.55–1.00)	0.84 (0.55–1.00)
	SM grade	1	0.69 (0.47–0.90)	0.69 (0.47–0.90)

SM Spetzler-Martin

intermodality agreement in our study was partly due to the relatively high spatial resolution of CS-TOF-MRA, which can facilitate the anatomical assessment of AVS, such as size of the nidus. Previous studies have suggested that CS-TOF-MRA offers a better signal-to-noise ratio [33, 37], which may also help the readers' evaluation of AVS consisted of small-caliber feeders or drainers.

This study has several limitations that warrant consideration. First, this was a retrospective study at a single center, and the number of patients was relatively small, so the results might be skewed. It should be noted that we did not included patients with micro AVM (i.e., nidus size ≦ 10 mm), which may be difficult to detect with TOF-MRA [14]. Second, analysis 1 included patients with intracranial pathologies other than AVS as controls, which represent a source of selection bias. Third, there are minor differences in imaging parameters between CS-TOF-MRA and PI-TOF-MRA in some patients, which may be a weakness of this study. Fourth, no optimization was performed for the current CS-TOF-MRA 6.5×. The current prototype CS-TOF-MRA had been developed after the

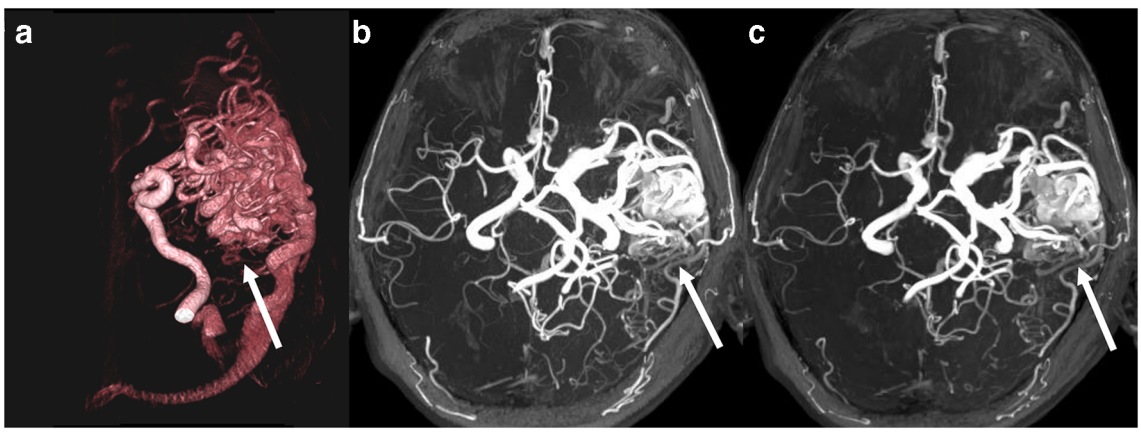

Fig. 2 A 50-year-old man with temporal AVM. DSA (**a**) of the left internal artery shows a large AVM (arrow) in the left temporal lobe. Frontal maximum intensity projection of PI-TOF-MR angiography (**b**) and CS-TOF-MR angiography (**c**) successfully visualize feeders, nidus, and drainer of AVM (arrow)

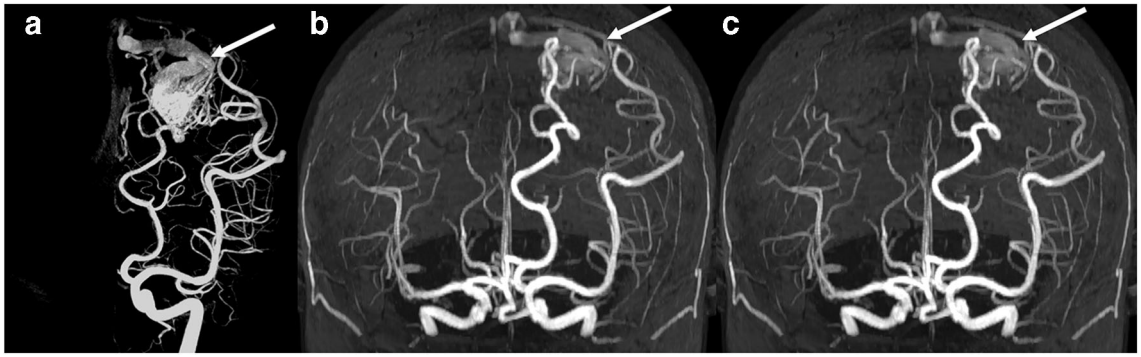

Fig. 3 A 19-year-old woman with left parietal AVM. Dyna-CT angiography (**a**), MIP images of PI-TOF-MRA (**b**), and CS-TOF-MRA (**c**) successfully delineate abnormal feeders from the left MCA and PCA, and nidus (arrow)

first prototype of CS-TOF-MRA used in the previous article [39], and the image quality had been interpreted as acceptable internally. Fifth, CS- and PI-TOF-MRA demonstrated moderate to good agreement with DSA in terms of venous reflux and SM grade of AVM. As shown in this study, it should be noted that TOF-MRA alone can be sometimes insufficient to evaluate cerebrovascular lesions, because TOF-MRA offers limited information about hemodynamics. TOF-MRA poorly delineates venous reflux, especially when the pattern is complex, that is, in any direction other than inferior to superior. TOF-MRA offers limited sensitivity and specificity for detecting drainage veins of AVM or venous reflux of AVF. Miyasaka et al. demonstrated that 6 of 27 drainage veins remained undetected on conventional TOF-MRA [18]. This may be due to the slow speed and complex directions of flow, leading to less inflow enhancement. In fact, several studies have shown the advantages of other advanced imaging techniques such as 4D-MRA, susceptibility-weighted imaging, and arterial spin labeling over TOF-MRA in the evaluation of AVS [13, 14, 18, 25, 27], at least in terms of concordance with DSA findings. These advanced sequences have specific advantages such as little effect of T1 shortening and detailed hemodynamic information. However, these advanced sequences also show limitations such as longer scanning time or limited availability, depending on vendors and research sites. Moreover, some techniques require contrast injection to evaluate flow

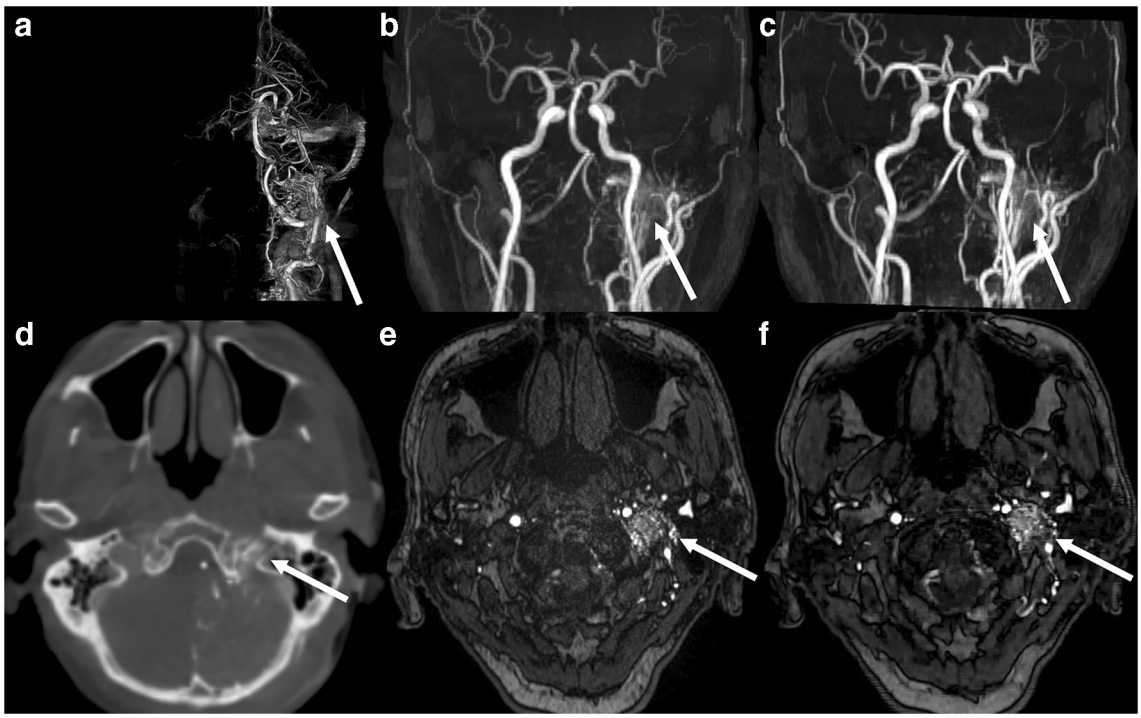

Fig. 4 A 68-year-old man with left anterior condylar confluence dural AVF. Volume rendering image of DSA (**a**), frontal maximum intensity projection of PI-TOF-MR angiography (**b**), and CS-TOF-MR angiography (**c**) visualize the dural AVF (arrow). Dyna-CT angiography (**d**) of the left VA demonstrates arteriovenous shunt from the dural branch of the left VA. Source images of PI-TOF-MRA (**e**) and CS-TOF-MRA (**f**) successfully delineate abnormal flow-related enhancement (arrow) surrounding the left internal jugular vein

dynamics [19, 21, 40]. Taking these characteristics into account, we believe these advanced image sequences should be used for selected patients with a high suspicion of AVS. On the other hand, regarding the reduced scanning time and large volume coverage, CS-TOF-MRA can be an efficient screening or monitoring tool for AVS with a reasonable concordance rate with DSA. Furthermore, the CS technique is used to either shorten the temporal footprint [30] or to increase spatial resolution within the same scan time [37], which may be applicable to further characterization of AVS.

In conclusion, CS-TOF-MRA yields comparable diagnostic performance in the detection and classification of AVM and AVS to that of PI-TOF-MRA, while reducing the scan time of under 2.5 min, without any degradation of image quality.

Acknowledgments We are grateful to Mr. Yuta Urushibata, MSci, and Mr. Katsutoshi Murata, MSci, Siemens Healthcare K. K. Japan, for protocol optimization.

Funding This work was supported by JSPS KAKENHI Grant Number JP18K07711, 19K17266, The Kyoto University Research Fund for Young Scientists (Start-Up) FY2020.

Compliance with ethical standards

Conflict of interest All authors declare that they have no conflict of interest except Michaela Schmidt, Christoph Forman, and Peter Speier who are employees of Siemens Healthcare GmbH.

Ethical approval All procedures performed in the studies involving human participants were in accordance with the ethical standards of the institutional and/or national research committee and with the 1964 Helsinki Declaration and its later amendments or comparable ethical standards.

Informed consent This retrospective study was approved by local institutional review boards and written informed consent was waived.

References

1. Wanke I, Rüfenacht DA (2015) The Dural AV-fistula (DAVF), the most frequent acquired vascular malformation of the central nervous system (CNS). Clin Neuroradiol 25(Suppl 2):325–332. https://doi.org/10.1007/s00062-015-0449-0
2. Unnithan A (2020) Overview of the current concepts in the management of arteriovenous malformations of the brain. Postgrad Med J 96(1134):212–220. https://doi.org/10.1136/postgradmedj-2019-137202
3. Jolink WM, van Dijk JM, van Asch CJ, de Kort GA, Algra A, Groen RJ, Rinkel GJ, Klijn CJ (2015) Outcome after intracranial haemorrhage from dural arteriovenous fistulae; a systematic review and case-series. J Neurol 262(12):2678–2683. https://doi.org/10.1007/s00415-015-7898-x
4. Ding D, Chen CJ, Starke RM, Kano H, Lee JYK, Mathieu D, Feliciano C, Rodriguez-Mercado R, Almodovar L, Grills IS, Kondziolka D, Barnett GH, Lunsford LD, Sheehan JP (2019) Risk of brain arteriovenous malformation hemorrhage before and after stereotactic radiosurgery. Stroke 50(6):1384–1391. https://doi.org/10.1161/strokeaha.118.024230
5. Brito A, Tsang ACO, Hilditch C, Nicholson P, Krings T, Brinjikji W (2019) Intracranial dural arteriovenous fistula as a reversible cause of dementia: case series and literature review. World Neurosurg 121:e543–e553. https://doi.org/10.1016/j.wneu.2018.09.161
6. Wang XC, Du YY, Tan Y, Qin JB, Wang L, Wu XF, Liang X, Zhang L, Li LN, Zhou X, Feng DP, Ma GL, Zhang H (2018) Brainstem congestion due to dural arteriovenous fistula at the craniocervical junction: case report and review of the literature. World Neurosurg 118:181–187. https://doi.org/10.1016/j.wneu.2018.06.243
7. Rocca G, Caputo F, Terranova C, Alice S, Ventura F (2019) Myelopathy due to intracranial dural arteriovenous fistula with perimedullary venous drainage: clinical and medico-legal aspects in a case of diagnostic pitfall. World Neurosurg 124:62–66. https://doi.org/10.1016/j.wneu.2018.12.150
8. Spetzler RF, Martin NA (1986) A proposed grading system for arteriovenous malformations. J Neurosurg 65(4):476–483. https://doi.org/10.3171/jns.1986.65.4.0476
9. Ding D, Ilyas A, Sheehan JP (2018) Contemporary management of high-grade brain arteriovenous malformations. Neurosurgery 65(CN_suppl_1):24–33. https://doi.org/10.1093/neuros/nyy107
10. Borden JA, Wu JK, Shucart WA (1995) A proposed classification for spinal and cranial dural arteriovenous fistulous malformations and implications for treatment. J Neurosurg 82(2):166–179. https://doi.org/10.3171/jns.1995.82.2.0166
11. Katsaridis V (2009) Treatment of dural arteriovenous fistulas. Curr Treat Options Neurol 11(1):35–40. https://doi.org/10.1007/s11940-009-0005-9
12. In 't Veld M, Fronczek R, Dos Santos MP, van Walderveen MAA, Meijer FJA, Willems PWA (2019) High sensitivity and specificity of 4D-CTA in the detection of cranial arteriovenous shunts. Eur Radiol 29(11):5961–5970. https://doi.org/10.1007/s00330-019-06234-4
13. Togao O, Hiwatashi A, Yamashita K, Momosaka D, Obara M, Nishimura A, Arimura K, Hata N, Iihara K, Van Cauteren M, Honda H (2019) Acceleration-selective arterial spin labeling MR angiography for visualization of brain arteriovenous malformations. Neuroradiology 61(9):979–989. https://doi.org/10.1007/s00234-019-02217-w
14. Arai N, Akiyama T, Fujiwara K, Koike K, Takahashi S, Horiguchi T, Jinzaki M, Yoshida K (2020) Silent MRA: arterial spin labeling magnetic resonant angiography with ultra-short time echo assessing cerebral arteriovenous malformation. Neuroradiology 62(4):455–461. https://doi.org/10.1007/s00234-019-02345-3
15. Tomura N, Saginoya T, Kokubun M, Horiuchi K, Watanabe Z (2019) Comparison of time-of-flight-magnetic resonance angiography from silent scan magnetic resonance angiography in depiction of arteriovenous malformation of the brain. J Comput Assist Tomogr 43(6):943–947. https://doi.org/10.1097/rct.0000000000000935
16. Lin YH, Wang YF, Liu HM, Lee CW, Chen YF, Hsieh HJ (2018) Diagnostic accuracy of CTA and MRI/MRA in the evaluation of the cortical venous reflux in the intracranial dural arteriovenous fistula DAVF. Neuroradiology 60(1):7–15. https://doi.org/10.1007/s00234-017-1948-2
17. Iryo Y, Hirai T, Kai Y, Nakamura M, Shigematsu Y, Kitajima M, Azuma M, Komi M, Morita K, Yamashita Y (2014) Intracranial dural arteriovenous fistulas: evaluation with 3-T four-dimensional MR angiography using arterial spin labeling. Radiology 271(1):193–199. https://doi.org/10.1148/radiol.13122670
18. Miyasaka T, Taoka T, Nakagawa H, Wada T, Takayama K, Myochin K, Sakamoto M, Ochi T, Akashi T, Kichikawa K (2012) Application of susceptibility weighted imaging (SWI) for

evaluation of draining veins of arteriovenous malformation: utility of magnitude images. Neuroradiology 54(11):1221–1227. https://doi.org/10.1007/s00234-012-1029-5
19. Li CQ, Hsiao A, Hattangadi-Gluth J, Handwerker J, Farid N (2018) Early hemodynamic response assessment of stereotactic radiosurgery for a cerebral arteriovenous malformation using 4D flow MRI. AJNR Am J Neuroradiol 39(4):678–681. https://doi.org/10.3174/ajnr.A5535
20. Komatsu K, Takagi Y, Ishii A, Kikuchi T, Yamao Y, Fushimi Y, Grinstead J, Ahn S, Miyamoto S (2018) Ruptured intranidal aneurysm of an arteriovenous malformation diagnosed by delay alternating with nutation for tailored excitation (DANTE)-prepared contrast-enhanced magnetic resonance imaging. Acta Neurochir 160(12):2435–2438. https://doi.org/10.1007/s00701-018-3713-7
21. Hadizadeh DR, von Falkenhausen M, Gieseke J, Meyer B, Urbach H, Hoogeveen R, Schild HH, Willinek WA (2008) Cerebral arteriovenous malformation: Spetzler-Martin classification at subsecond-temporal-resolution four-dimensional MR angiography compared with that at DSA. Radiology 246(1):205–213. https://doi.org/10.1148/radiol.2453061684
22. Wu CX, Ma L, Chen XZ, Chen XL, Chen Y, Zhao YL, Hess C, Kim H, Jin HW, Ma J (2018) Evaluation of angioarchitectural features of unruptured brain arteriovenous malformation by susceptibility weighted imaging. World Neurosurg 116:e1015–e1022. https://doi.org/10.1016/j.wneu.2018.05.151
23. Azuma M, Hirai T, Shigematsu Y, Kitajima M, Kai Y, Yano S, Nakamura H, Makino K, Iryo Y, Yamashita Y (2015) Evaluation of intracranial dural arteriovenous fistulas: comparison of unenhanced 3T 3D time-of-flight MR angiography with digital subtraction angiography. Magn Reson Med Sci 14(4):285–293. https://doi.org/10.2463/mrms.2014-0120
24. Kwon BJ, Han MH, Kang HS, Chang KH (2005) MR imaging findings of intracranial dural arteriovenous fistulas: relations with venous drainage patterns. AJNR Am J Neuroradiol 26(10):2500–2507
25. Schubert T, Clark Z, Sandoval-Garcia C, Zea R, Wieben O, Wu H, Turski PA, Johnson KM (2018) Non contrast, pseudo-continuous arterial spin labeling and accelerated 3-dimensional radial acquisition intracranial 3-dimensional magnetic resonance angiography for the detection and classification of intracranial arteriovenous shunts. Investig Radiol 53(2):80–86. https://doi.org/10.1097/rli.0000000000000411
26. Yu S, Yan L, Yao Y, Wang S, Yang M, Wang B, Zhuo Y, Ai L, Miao X, Zhao J, Wang DJ (2012) Noncontrast dynamic MRA in intracranial arteriovenous malformation (AVM), comparison with time of flight (TOF) and digital subtraction angiography (DSA). Magn Reson Imaging 30(6):869–877. https://doi.org/10.1016/j.mri.2012.02.027
27. Hodel J, Leclerc X, Kalsoum E, Zuber M, Tamazyan R, Benadjaoud MA, Pruvo JP, Piotin M, Baharvahdat H, Zins M, Blanc R (2017) Intracranial arteriovenous shunting: detection with arterial spin-labeling and susceptibility-weighted imaging combined. AJNR Am J Neuroradiol 38(1):71–76. https://doi.org/10.3174/ajnr.A4961
28. Lin YH, Lin HH, Liu HM, Lee CW, Chen YF (2016) Diagnostic performance of CT and MRI on the detection of symptomatic intracranial dural arteriovenous fistula: a meta-analysis with indirect comparison. Neuroradiology 58(8):753–763. https://doi.org/10.1007/s00234-016-1696-8
29. Okuchi S, Fushimi Y, Okada T, Yamamoto A, Kikuchi T, Yoshida K, Miyamoto S, Togashi K (2019) Visualization of carotid vessel wall and atherosclerotic plaque: T1-SPACE vs. compressed sensing T1-SPACE. Eur Radiol 29(8):4114–4122. https://doi.org/10.1007/s00330-018-5862-8
30. Yokota Y, Fushimi Y, Okada T, Fujimoto K, Oshima S, Nakajima S, Fujii T, Tanji M, Inagaki N, Miyamoto S, Togashi K (2020) Evaluation of image quality of pituitary dynamic contrast-enhanced MRI using time-resolved angiography with interleaved stochastic trajectories (TWIST) and iterative reconstruction TWIST (IT-TWIST). J Magn Reson Imaging 51(5):1497–1506. https://doi.org/10.1002/jmri.26962
31. Yamamoto T, Okada T, Fushimi Y, Yamamoto A, Fujimoto K, Okuchi S, Fukutomi H, Takahashi JC, Funaki T, Miyamoto S, Stalder AF, Natsuaki Y, Speier P, Togashi K (2018) Magnetic resonance angiography with compressed sensing: an evaluation of moyamoya disease. PLoS One 13(1):e0189493. https://doi.org/10.1371/journal.pone.0189493
32. Lin Z, Zhang X, Guo L, Wang K, Jiang Y, Hu X, Huang Y, Wei J, Ma S, Liu Y, Zhu L, Zhuo Z, Liu J, Wang X (2019) Clinical feasibility study of 3D intracranial magnetic resonance angiography using compressed sensing. J Magn Reson Imaging 50(6):1843–1851. https://doi.org/10.1002/jmri.26752
33. Fushimi Y, Okada T, Kikuchi T, Yamamoto A, Yamamoto T, Schmidt M, Yoshida K, Miyamoto S, Togashi K (2017) Clinical evaluation of time-of-flight MR angiography with sparse undersampling and iterative reconstruction for cerebral aneurysms. NMR Biomed 30(11). https://doi.org/10.1002/nbm.3774
34. Lustig M, Donoho D, Pauly JM (2007) Sparse MRI: the application of compressed sensing for rapid MR imaging. Magn Reson Med 58(6):1182–1195. https://doi.org/10.1002/mrm.21391
35. Lu SS, Qi M, Zhang X, Mu XH, Schmidt M, Sun Y, Forman C, Speier P, Hong XN (2018) Clinical evaluation of highly accelerated compressed sensing time-of-flight MR angiography for intracranial arterial stenosis. AJNR Am J Neuroradiol 39(10):1833–1838. https://doi.org/10.3174/ajnr.A5786
36. Zhang X, Cao YZ, Mu XH, Sun Y, Schmidt M, Forman C, Speier P, Lu SS, Hong XN (2020) Highly accelerated compressed sensing time-of-flight magnetic resonance angiography may be reliable for diagnosing head and neck arterial steno-occlusive disease: a comparative study with digital subtraction angiography. Eur Radiol 30:3059–3065. https://doi.org/10.1007/s00330-020-06682-3
37. Demerath T, Bonati L, El Mekabaty A, Schubert T (2020) High-resolution compressed-sensing time-of-flight MRA in a case of acute ICA/MCA dissection. Neuroradiology. 62:753–756. https://doi.org/10.1007/s00234-020-02395-y
38. Jagadeesan BD, Delgado Almandoz JE, Moran CJ, Benzinger TL (2011) Accuracy of susceptibility-weighted imaging for the detection of arteriovenous shunting in vascular malformations of the brain. Stroke 42(1):87–92. https://doi.org/10.1161/STROKEAHA.110.584862
39. Yamamoto T, Fujimoto K, Okada T, Fushimi Y, Stalder AF, Natsuaki Y, Schmidt M, Togashi K (2016) Time-of-flight magnetic resonance angiography with sparse undersampling and iterative reconstruction: comparison with conventional parallel imaging for accelerated imaging. Investig Radiol 51(6):372–378. https://doi.org/10.1097/rli.0000000000000221
40. Denby CE, Chatterjee K, Pullicino R, Lane S, Radon MR, Das KV (2020) Is four-dimensional CT angiography as effective as digital subtraction angiography in the detection of the underlying causes of intracerebral haemorrhage: a systematic review. Neuroradiology 62(3):273–281. https://doi.org/10.1007/s00234-019-02349-z